Journal of Materials Chemistry C

ROYAL SOCIETY OF CHEMISTRY

PAPER

View Article Online
View Journal

Cite this: DOI: 10.1039/d5tc03602j

Enhanced exciton luminescence and fast scintillation potential in Sr^{2+}-activated $CsPbCl_3$ single crystals

Andrii Pushak,[a] Oleksandr Pidhornyi,[a] Yaroslav Chornodolskyy,[a] Taras Malyi,[a] Taras Demkiv, *[a] Oleh Antonyak,[a] Volodymyr Stakhura,[a] Volodymyr Salapak, [b] Roman Gamernyk,[a] Oleh Bovgyra,[a] Anatoliy Zelinskiy, [a] Yevheniia Smortsova,[c] Aleksei Kotlov[c] and Anatoliy Voloshinovskii[a]

Single crystals of pristine and Sr^{2+}-activated $CsPbCl_3$ were grown using the vertical Stockbarger technique, and their luminescence properties were investigated. Under excitation with synchrotron-radiation photons of 7.75 eV, which substantially exceeds the band gap energy, the pristine crystals exhibit a pronounced excitonic emission band with a maximum at ~417 nm, whereas Sr^{2+}-activated crystals reveal the emergence of additional exciton-like bands in the near edge region, accompanied by a tendency of the edge emission to shift toward higher energies. The activated crystals also demonstrate a pronounced enhancement of luminescence intensity, reaching nearly a tenfold increase for $CsPbCl_3$:Sr (1 mol%). The additional exciton-like emission band Sr^{2+}-activated crystals may originate from excitons localized at defect-related sites. The average decay time constants of the excitonic emission bands in both the pristine and the activated crystals are approximately 500 ps at 10 K and 60 ps at 77 K. The temperature evolution of luminescence intensity is interpreted in terms of electron escape beyond the Onsager sphere, whose radius decreases with increasing temperature, whereas the temperature-induced changes in the decay time constants are attributed to thermally assisted exciton dissociation. The pronounced enhancement of near band edge luminescence intensity in Sr^{2+}-activated $CsPbCl_3$ crystals highlights their potential for application as fast scintillators.

Received 2nd October 2025,
Accepted 15th February 2026

DOI: 10.1039/d5tc03602j

rsc.li/materials-c

1. Introduction

The defect tolerance of halide perovskites opens a new pathway for enhancing their functional properties. This effect is particularly pronounced in the luminescence characteristics of halide perovskite nanocrystals activated with alkaline-earth, 3d-transition, and even lanthanide cations.[1–3] Remarkable results have been demonstrated for the luminescence of $CsPbCl_3$ nanocrystals doped with metal cations, such as cadmium and magnesium, where the photoluminescence quantum yield increased from 2% to 100%.[4,5] The primary factors underlying the enhancement of excitonic luminescence intensity of nanoparticles are commonly attributed to the improved structural quality of the perovskite lattice and the passivation of surface defects.[3] This pronounced trend of excitonic luminescence enhancement in doped perovskite nanocrystals may be innovative not only for the development of composite nanocrystal-based scintillators[6,7] but also for single-crystal perovskite scintillators.[8]

Despite repeated attempts to evaluate the scintillation efficiency of lead halide single crystals,[9] the scintillation yield of these materials remains under investigation and refinement.[10] Metal cation activation offers a promising route to improve the scintillation performance of perovskite single crystals, as it has been shown to effectively enhance the photoluminescence quantum yield in perovskite nanocrystals. A representative example was reported in ref. 8 where $CsPbCl_3$ single crystals activated with 4 mol% $CdCl_2$ exhibited more than an order of magnitude increase in near edge luminescence intensity, together with a decay constant of ~0.4 ns. The enhancement factor in $CsPbCl_3$:Cd single crystals is, however, smaller than in analogous nanocrystals, where the luminescence intensity increases by nearly two orders of magnitude. This difference highlights the dominant role of surface passivation in nanocrystals, whereas in single crystals the surface contribution is not critical for luminescence quenching. Instead, the improvement in single crystals is primarily linked to the ordering of the

[a] Ivan Franko National University of Lviv, 1 Universytetska Str., 79000, Lviv, Ukraine. E-mail: taras.demkiv@lnu.edu.ua
[b] Ukrainian National Forestry University, 103 Gen. Chuprynky St., 79057, Lviv, Ukraine
[c] Deutsches Elektronen-Synchrotron DESY, Notkestr. 85, 22607, Hamburg, Germany

perovskite lattice, which contains numerous anionic and cationic defects acting as exciton traps. Furthermore, single crystals enable direct analysis of the impact of activation on exciton dynamics, unlike nanocrystals, where excitonic emission arises from the superposition of bands originating from an ensemble of different-sized particles. The size distribution of nanocrystals, together with varying manifestations of the quantum confinement effect, results in a structureless luminescence band with a full width at half maximum broader than that of the excitonic band observed in single crystals.

In this study, we aim to elucidate the influence of Sr^{2+} doping on the near edge luminescence efficiency of $CsPbCl_3$ single crystals, by comparing it with the reported results for $CsPbCl_3$:Cd.[8] Unlike Cd^{2+} activation, where the 4d states contribute to the conduction band, Sr^{2+} ions introduce not only 3d states but also 5s states into the conduction band. In the case of hybridization with the Pb 6p states, this may lead to a widening of the perovskite band gap and an increased probability of Cl^- 3p → Sr^{2+} 5s, 3d transitions. Another important distinction between cadmium and strontium is associated with their different ionic radii: 1.09 Å for Cd^{2+} and 1.32 Å for Sr^{2+} in octahedral coordination, compared to 1.33 Å for Pb^{2+}. Since the ionic radius of Sr^{2+} is close to that of Pb^{2+}, it is reasonable to assume that its incorporation into the matrix will lead to the formation of fewer luminescence-quenching defects.

To clarify the scintillation mechanisms, we investigated the luminescence properties of pristine and Sr^{2+}-activated $CsPbCl_3$ single crystals under band-to-band excitation by synchrotron radiation quanta with an energy of $h\nu$ = 7.75 eV (λ = 160 nm). This excitation energy significantly exceeds the band gap of the crystal (E_g = 2.97 eV), thereby providing conditions close to those realized in scintillation processes.

2. Experimental

Single crystals of the halide perovskite $CsPbCl_3$ were grown from the melt using the Stockbarger technique. CsCl of 99.99% purity and $PbCl_2$, which was preliminarily purified by multiple zone melting, were used as starting materials. $SrCl_2$ of 99.99% purity was employed for activation. The precursor components in stoichiometric ratios were loaded into a quartz ampoule with a diameter of 10 mm, which was evacuated for 8 h at 300 °C. The sealed ampoule was placed into a high-temperature furnace at a temperature slightly above the melting point of the starting mixture. After complete melting, the ampoule was lowered through a region with a controlled temperature gradient at a rate of 1 mm h^{-1}. Upon completion of crystal growth, the ampoule was kept at 300 °C for 10 h, followed by cooling to room temperature over 24 h. For the growth of activated single crystals, the dopant was added in excess relative to the stoichiometric composition, and its concentration is indicated by its amount in the initial mixture. The pristine $CsPbCl_3$ and Sr-doped $CsPbCl_3$–$SrCl_2$ (0.5 mol%, 1 mol%, and 5 mol%) single crystals were grown. The concentration of strontium in the crystals, according to the results of X-ray fluorescence analysis, is close to that added to the starting material (Fig. S1 and Table S1).

Luminescence measurements under synchrotron excitation were performed at the PETRA III P66 beamline of DESY.[11] Luminescence spectra were recorded using a Kymera 328i spectrograph with a spectral slit width of 2 Å and detected by a Newton 920 CCD camera. The excitation radiation was selected by a McPherson primary 2 m normal-incidence monochromator with a spectral slit width of 4 Å in a 15° mounting, covering the UV and VUV spectral range from 3.7 eV to 40 eV.

Time-resolved luminescence measurements were carried out using the time-correlated single-photon counting technique, with the luminescence intensity being recorded with a Hamamatsu R3809U-50 MCP-PMT detector. The decay time constant of the synchrotron excitation pulse, taking into account the time response of the photomultiplier, was 50 ps.

Temperature-dependent luminescence measurements in the range of 10–300 K were performed using a helium-flow cryostat. Measurements of the luminescence properties were performed from freshly cleaved crystal surfaces.

3. Results and discussion

3.1. Luminescent properties of $CsPbCl_3$:Sr at 10 K

3.1.1. Luminescence spectra. The luminescence spectra dynamics of $CsPbCl_3$ single crystals as a function of Sr^{2+} ion concentration at 10 K are presented in Fig. 1. This figure facilitates a direct comparison of the luminescence intensities among the samples. The maximum luminescence intensity of the activated crystals is observed at the Sr^{2+} concentration of 1 mol% (Fig. 1, inset). At this concentration, the luminescence intensity of the $CsPbCl_3$:Sr^{2+} (1 mol%) is nearly one order of magnitude higher than that of the pristine crystal. One possible reason for this enhancement is the improved ordering of the lattice due to a reduction in the number of cationic and anionic vacancies, which act as quenching centers for excitonic

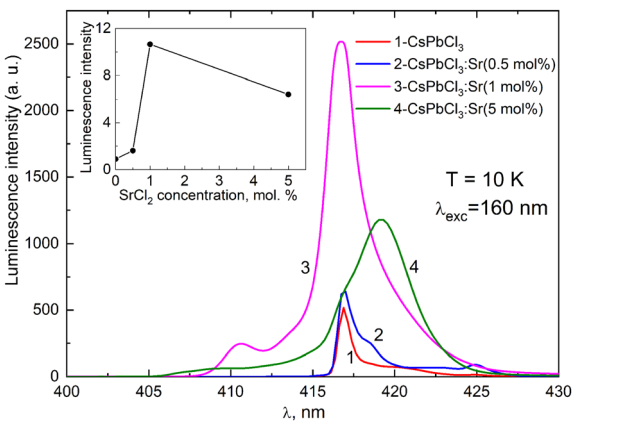

Fig. 1 Luminescence spectra of pristine $CsPbCl_3$ single crystals (curve 1) and $SrCl_2$-doped crystals (0.5 mol% – curve 2; 1 mol% – curve 3; 5 mol% – curve 4) at T = 10 K. Excitation: $h\nu_{exc}$ = 7.75 eV (λ_{exc} = 160 nm). Inset: Dependence of the luminescence intensity on the $SrCl_2$ dopant concentration.

luminescence. Chlorine vacancies with an energy of 0.7 eV[12] serve as traps for the electron component of the exciton. The additional incorporation of chlorine during $SrCl_2$ doping helps to reduce the number of chlorine vacancies. In parallel, Sr^{2+} incorporation increases the formation energy of chlorine vacancies[13] and reduces the number of Pb^{2+} vacancies (see the SI, Chapter 3: Impurity formation energies in Sr-doped $CsPbCl_3$ crystals).

Computational results show that the formation energy for a chlorine vacancy is 2.79 eV for pristine $CsPbCl_3$ and increases to 5.46–6.68 eV in Sr-doped $CsPbCl_3$, depending on the relative position of the chlorine vacancy to the Sr dopant (see the SI, Chapter 5: Influence of strontium doping on the formation energy of chlorine vacancies). A substantial increase in formation energy of a chlorine vacancy indicates that isovalent Sr substitution stabilizes the lattice and suppresses the formation of anion vacancies. Therefore, Sr^{2+} doping contributes to a reduced concentration of chlorine vacancies, thereby stabilizing the lattice and decreasing the number of exciton-trapping defects.

The luminescence spectra of pristine and Sr^{2+}-doped $CsPbCl_3$ samples, normalized to their respective intensities, are shown in Fig. 2. Normalized spectra allow for a clearer observation of spectral structure changes as a function of dopant concentration. The luminescence of the pristine $CsPbCl_3$ sample (Fig. 2, curve 1) exhibits a narrow emission band at 416.9 nm, which is commonly attributed to free exciton emission.[8,14,15] In addition, as shown in Fig. 3a and Table 1, based on the decomposition of the luminescence band contour into individual components, several narrow emission bands with a linewidth of approximately 10 meV are observed. These bands can be interpreted as exciton-like luminescence associated with excitons localized on crystal lattice defects. Similar narrow exciton-like emission has also been reported for pure $CsPbCl_3$[14] and $CsPbCl_3$–Cd crystals.[8]

The addition of 0.5 mol% $SrCl_2$ to $CsPbCl_3$ (Fig. 2, curve 2) results in a slight increase in the intensity of the excitonic emission at 416.9 nm and of the localized exciton at 425 nm.

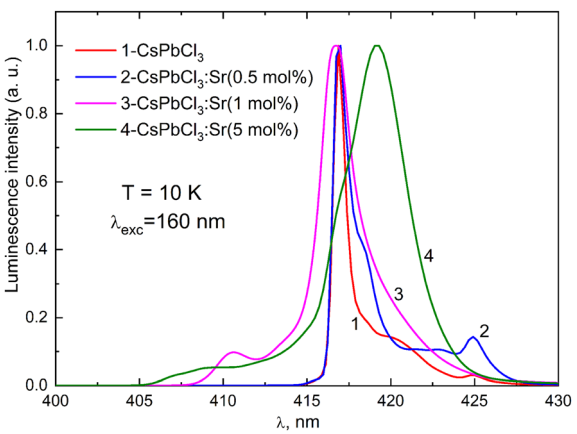

Fig. 2 Normalized luminescence spectra of pristine $CsPbCl_3$ single crystals (curve 1) and $SrCl_2$-doped crystals (0.5 mol% – curve 2; 1 mol% – curve 3; 5 mol% – curve 4) at T = 10 K. Excitation: $h\nu_{exc}$ = 7.75 eV (λ_{exc} = 160 nm).

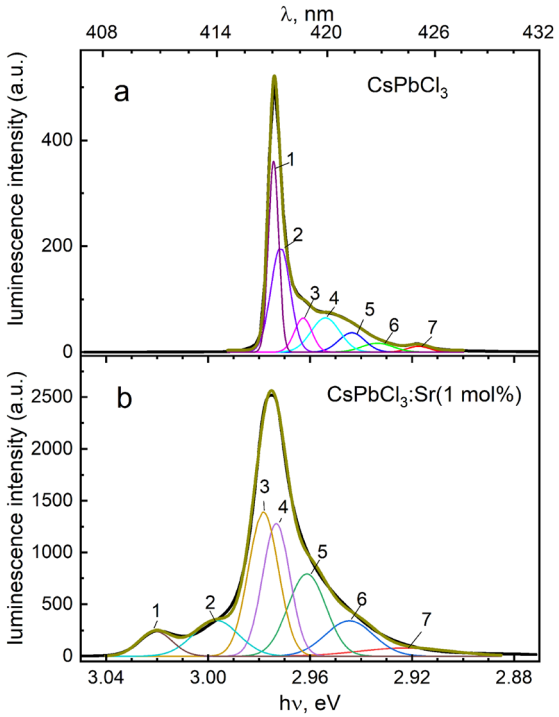

Fig. 3 Decomposition of the luminescence band of the pure $CsPbCl_3$ crystal (a) and 1 mol% $SrCl_2$ doped $CsPbCl_3$ crystal (b) at a temperature of 10 K.

Table 1 The decomposition parameters of the $CsPbCl_3$ and the $CsPbCl_3$–$SrCl_2$(1 mol %) near-edge luminescence spectrum at a temperature of 10 K. E_{max} is the position of the maximum of the band, and ΔE represents the half-width of the band

Peak number	E_{max}, eV	ΔE, meV	E_{max}, eV	ΔE, meV
$CsPbCl_3$			$CsPbCl_3$–$SrCl_2$(1 mol%)	
1	2.974	4.01	3.021	13.1
2	2.972	7.60	2.997	17.9
3	2.963	6.84	2.978	11.8
4	2.954	11.20	2.973	10.8
5	2.944	10.20	2.961	14. 9
6	2.934	12.20	2.945	19.0
7	2.917	8.90	2.923	36.3

Striking changes in the luminescence spectra are observed for $CsPbCl_3$:Sr^{2+} (1 mol%) crystals (Fig. 2, curve 3): (i) the emission band maximum shifts slightly toward higher energy, reaching 416.7 nm; (ii) the band broadens, which may result from the superposition of several narrow emission bands associated with localized excitons; (iii) the excitonic emission intensity at the maximum increases by a factor of six, and a new emission band appears at 410.6 nm, which may indicate a reconstruction of the band structure in $CsPbCl_3$.

Increasing the Sr^{2+} concentration to 5 mol% (Fig. 2, curve 4) further shifts the edge of the near edge luminescence toward shorter wavelengths, reaching 405 nm, while the maximum luminescence intensity corresponds to the spectral region associated with localized exciton emission ($\lambda > 417$ nm).

As in the case of a pure crystal, the contour of the luminescence band of the activated crystal can be decomposed into separate narrow components (Fig. 3b and Table 1). At present, the identification of such bands in $CsPbCl_3$ is generally limited to the terms free or localized excitons, without unambiguous attribution to specific defect types. Intrinsic lattice defects, such as chlorine, lead, or cesium vacancies, are not considered as exciton localization centers, since they represent deep charged states with energies of 0.15–0.7 eV and primarily act as carrier traps, resulting in quenching of excitonic luminescence.

The luminescence observed upon Sr activation of $CsPbCl_3$ enables us to propose a defect model responsible for exciton localization. Incorporation of Sr^{2+} into the lattice results in the formation of an isovalent neutral defect, in which Sr^{2+} substitutes Pb^{2+} (Sr_Pb^0). The formation of this defect gives rise to a local potential well where an exciton can be trapped. The number of quasi-stationary excitonic states (emission bands) is associated with different local configurations of the same isovalent defect (Sr occupying the Pb site), corresponding to a set of closely spaced potential minima. We attribute the observed bands to excitons weakly localized at the isovalent Sr_Pb^0 defect, where Sr^{2+} substitutes Pb^{2+} without introducing deep electronic levels in the band gap. The Sr substitution locally distorts the $PbCl_6$ octahedra and stabilizes several quasi-equilibrium lattice configurations. Each configuration supports a specific exciton–phonon coupled state characterized by a distinct localization depth.

Considering the nature of the defects responsible for the exciton-like luminescence in $CsPbCl_3$:Sr, it can be assumed that additional exciton-like bands observed in pure $CsPbCl_3$ crystals are related to excitons localized at uncontrolled extrinsic defects.

Theoretical calculations allow the high-energy shift of the absorption edge in $CsPbCl_3$:Sr^{2+} crystals to be interpreted as a result of the mixing of Sr 5s- and 3d-states with the Pb p-states at the bottom of the conduction band.[13] This mixing renders transitions from the Cl 3p valence states to the conduction band s- and d- states dipole-allowed, which may enhance the intensity of near edge luminescence. The evolution of the band structure parameters and density states upon Sr incorporation is presented in Fig. S2 and S3.

The overall impact of doping on the luminescent characteristics of the $CsPbCl_3$:Sr crystal can be highlighted. The introduction of Sr^{2+} leads to a spectral shift of the near edge luminescence toward higher energies, and additional emission bands can be attributed to excitons localized at lattice defects. Considering the influence of dopants on the perovskite structure, in particular the reduction of anionic vacancies,[12,13] as well as analogous effects observed in nanocrystals and in $CsPbCl_3$:Cd,[8] it can be concluded that Sr^{2+} doping improves the structural ordering of the perovskite lattice.

In $CsPbCl_3$ crystals with 1 mol% Sr^{2+} (Fig. 1, curve 3), the integrated luminescence intensity increases by nearly one order of magnitude. This is a promising result for the use of $CsPbCl_3$ crystals as scintillators. Theoretical estimates of the light yield of $CsPbCl_3$ crystals reach 133 000 photons per MeV. Recent measurements[10] report a light yield of 2200 photons per MeV under X-ray excitation at 40 keV. Taking these results into account, it can be expected that the light yield of doped crystals, particularly $CsPbCl_3$:Cd[8] and $CsPbCl_3$:Sr, may reach 22 000 photons per MeV, highlighting the potential of doped crystals as fast scintillators at low temperatures.

3.1.2. Luminescence decay curves at 10 K. The luminescence decay curves of pristine $CsPbCl_3$ and Sr-doped $CsPbCl_3$ crystals are shown in Fig. 4. These curves provide information not only on the quantitative parameters of the decay kinetics but also on the role of defects in shaping the scintillation response. The decay curve of the excitonic emission ($\sim$417 nm) in the pristine $CsPbCl_3$ crystal can be described by an average decay time constant of τ_{av} = 493 ps (Table 2), calculated using the formula

$$\tau_{av} = \frac{\sum_i A_i \tau_i^2}{\sum_i A_i \tau_i}, \quad (1)$$

where τ_i are the decay time constants of the individual components, and A_i are the corresponding amplitudes of these components in the decay curve decomposition.

In $CsPbCl_3$:Sr (0.5 mol%), the luminescence pulse width increases significantly to 1 ns (Fig. 4, curve 2) compared to

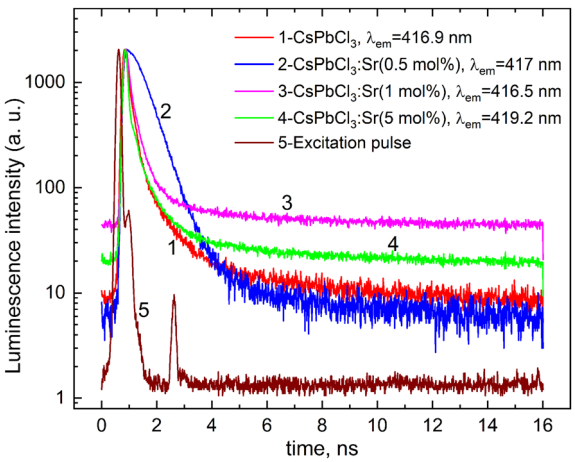

Fig. 4 Luminescence decay curves of pristine $CsPbCl_3$ single crystals (curve 1) and $SrCl_2$-doped crystals (curve 2 – 0.5 mol%; curve 3 – 1 mol%; curve 4 – 5 mol%) at T = 10 K. Excitation pulse profile – curve 5. Excitation: $h\nu_{exc}$ = 7.75 eV (λ_{exc} = 160 nm).

Table 2 Decay time constants of near edge excitonic luminescence in $CsPbCl_3$ and $CsPbCl_3$:Sr (T = 10 K) and 5 mol% remain close to that of pristine $CsPbCl_3$, approximately 500 ps

Crystal	Maxima of band (nm)	A_1	τ_1 (ps)	A_2	τ_2 (ps)	τ_{av} (ps)
$CsPbCl_3$	416.9	1896	191	146	1147	493
	420.7	1688	183	145	1290	601
$CsPbCl_3$:Sr (0.5 mol%)	417	1156	534			534
	424	1086	593			593
$CsPbCl_3$:Sr (1 mol %)	416.5	1877	204	162	1060	469
	410.6	1886	161	41	1931	527
$CsPbCl_3$:Sr (5 mol %)	419.3	1884	193	218	887	434
	409	1941	159	31	1820	416

0.2 ns for pristine $CsPbCl_3$ (Fig. 4, curve 1), while the decay time constant remains nearly unchanged at τ_1 = 534 ps, similar to that of the pristine crystal (τ_{av} = 493 ps). The observed broadening of the pulse for 0.5 mol% Sr^{2+} can be attributed to the formation of shallow traps. The processes involving multiple capture and release events from these shallow traps may account for the pulse broadening. Further increase in Sr^{2+} concentration (1 mol%, 5 mol%) leads to a restoration of the scintillation pulse width, which may be associated with the disappearance of shallow traps. At the same time, the scintillation pulse exhibits a relatively long decay component that contributes to the background signal at longer times. The increase in the background level can be associated with the presence of deeper traps, whose slow carrier release gives rise to a long-lived tail in the decay curves. The average decay time values for $CsPbCl_3$:Sr at 1 mol% and 5 mol% remain close to that of pristine $CsPbCl_3$, approximately 500 ps.

As emphasized, the near-edge luminescence comprises a series of narrow exciton-like bands, with one dominant band that can be tentatively assigned to free exciton emission. Comparing the decay time constants of the excitonic band and the exciton-like luminescence can provide additional insight into their origin. The fast decay components, τ_1, of the pristine $CsPbCl_3$ crystal for the 416.9 nm exciton band and the longest-wavelength band at 420.7 nm, with values of τ_1 = 191 ps and τ_1 = 183 ps, respectively (Fig. 5a and Table 2), may indicate a similar nature of these luminescence bands. For $CsPbCl_3$:Sr (1 mol%), the decay curves of the most intense band at 416.5 nm and the highest-energy band at 410.6 nm (Fig. 5c) reveal τ_1 = 204 ps and τ_1 = 161 ps, respectively (Table 2). This difference in decay time constants may suggest a slightly different origin of these bands. A similar distinction is observed for the bands at 419.3 nm and 409 nm (193 ps and 159 ps, respectively) for 5 mol% Sr^{2+} (Fig. 5d, Table 2).

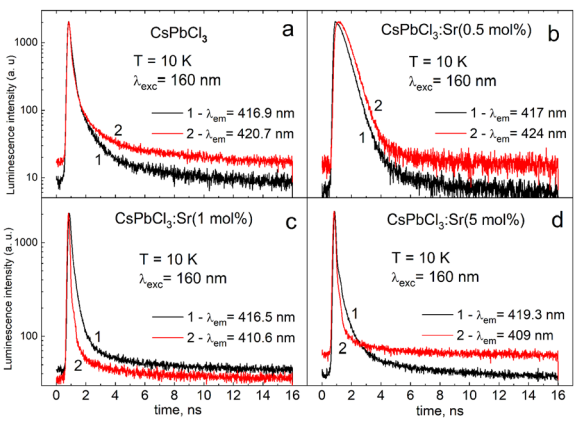

Fig. 5 Luminescence decay curves for different luminescence bands of near edge luminescence in $CsPbCl_3$ (a), $CsPbCl_3$:Sr (0.5 mol%) (b), $CsPbCl_3$:Sr (1 mol%) (c), and $CsPbCl_3$:Sr (5 mol%) (d). T = 10 K. Excitation: $h\nu_{exc}$ = 7.75 eV (λ_{exc} = 160 nm).

3.2. Temperature dependence of luminescence parameters

3.2.1. Luminescence spectra. The temperature dependent luminescence spectra of the pristine $CsPbCl_3$ sample and the $CsPbCl_3$:Sr (1 mol%) sample are presented in Fig. 5 and 6. The $CsPbCl_3$:Sr (1 mol%) sample was chosen for comparison with $CsPbCl_3$ as it demonstrates the largest increase in the integrated luminescence intensity upon Sr^{2+} doping. In addition, we restrict our analysis to the temperature dependence of the integral luminescence intensity, since this quantity is directly relevant for scintillation detectors, where the total emitted light yield is the key parameter.

For the pristine sample, the luminescence quenching correlates with a decrease in the excitonic luminescence intensity (Fig. 6). In the Sr^{2+}-doped $CsPbCl_3$ (1 mol%) sample (Fig. 7), luminescence quenching occurs differently across various spectral regions. Upon increasing the temperature, the bands in the short-wavelength region of the spectrum exhibit a slower rate of luminescence quenching (Fig. 7b and Fig. S4).

The temperature dependences of the luminescence intensity for the $CsPbCl_3$ and $CsPbCl_3$:Sr (1 mol%) samples are shown in Fig. 8. The quenching of the integrated luminescence is approximated using the Mott formula with two activation barriers,

$$I(T) = \frac{I_0}{\left(1 + \sum_i A_i \cdot \exp(-E_i/kT)\right)}, \qquad (2)$$

where i = 1 and 2, and E_1 and E_2 are the activation energies for luminescence quenching. For the pristine crystal, E_1 = 5.1 meV and E_2 = (39 ± 3) meV. For the $CsPbCl_3$:Sr (1 mol%) crystal, E_1 = 4.7 meV and E_2 = (30 ± 3) meV. Similar values of the

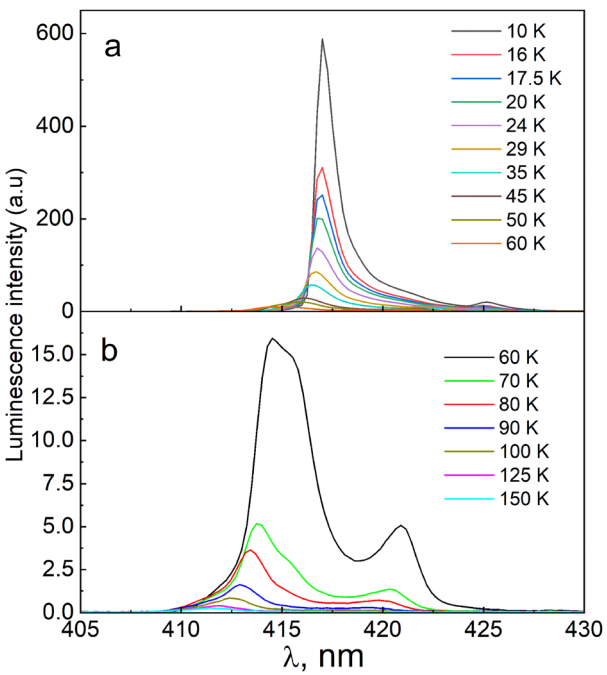

Fig. 6 Luminescence spectra of the pristine $CsPbCl_3$ single crystal for the temperature ranges 10–60 K (a) and 60–150 K (b).

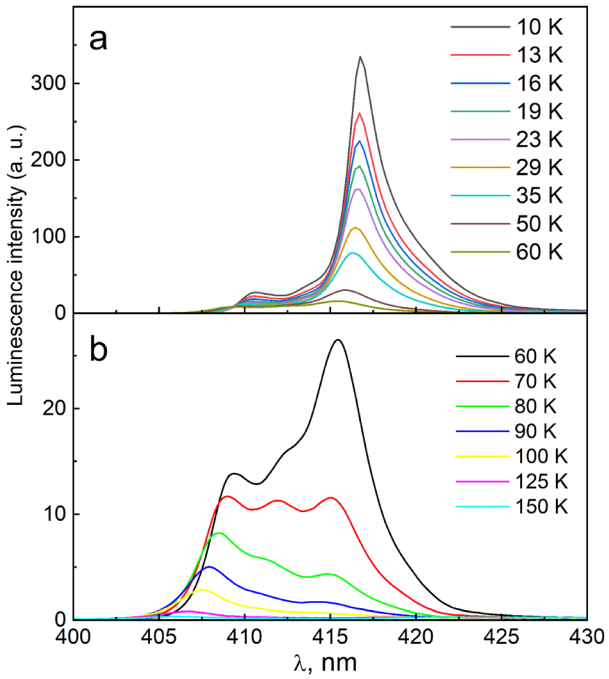

Fig. 7 Luminescence spectra of the $CsPbCl_3$:Sr crystal (1 mol%) for the temperature ranges 10–60 K (a) and 60–150 K (b).

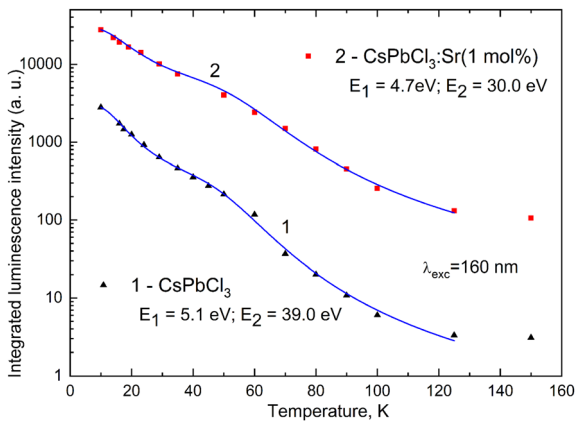

Fig. 8 Temperature dependence of the integrated luminescence intensity of the $CsPbCl_3$ single crystal (curve 1) and the $CsPbCl_3$:Sr (1 mol%) single crystal (curve 2). Excitation: $h\nu_{exc}$ = 7.75 eV (λ_{exc} = 160 nm).

activation barrier for exciton quenching (~30 meV) in the pristine crystal are also reported in ref. 9 and 14. In particular, ref. 9 reports that in pristine $CsPbCl_3$ single crystals the authors distinguish five luminescence bands, for which the activation energy for quenching of excitonic emission lies in the range from 8.4 meV to 37.9 meV.

The obtained activation energies for luminescence quenching do not correspond to the exciton binding energy in $CsPbCl_3$. Based on the positions of the excitonic absorption bands, the exciton binding energy is estimated to be 64 meV.[16] The difference between the activation energies derived from luminescence quenching and the exciton binding energy can be explained by analyzing the relationship between the electron thermalization length and the Onsager radius (R_{Ons}).

Under high-energy band-to-band excitation at 160 nm (7.75 eV), a geminate electron–hole pair is generated with the electron having a kinetic energy of 4.7 eV in the conduction band. The electron loses its energy through scattering on electrons and lattice phonons. The average electron thermalization length $\langle r^2\rangle^{1/2}$ during scattering on phonons can reach tens to hundreds of nanometers.[17–19]

To estimate the efficiency of recombination of the geminate pairs, the electron thermalization length $\langle r^2\rangle^{1/2}$ should be compared with the Onsager radius. If the thermalization length exceeds the Onsager radius, there is a certain probability that charge carriers will be trapped at defects, which leads to exciton luminescence quenching. The Onsager radius is defined as the distance at which the magnitude of the Coulomb interaction between the electron and the hole approximately equals the thermal energy k_BT. In $CsPbCl_3$, according to the formula

$$R_{Ons} = \frac{e^2}{(4\pi\varepsilon_0\varepsilon k_B T)}, \quad (3)$$

where ε = 6.5 is the static dielectric permittivity,[16] the Onsager radius is 310 nm at T = 10 K, 100 nm at 45 K, and 30 nm at 150 K. Typical thermalization lengths for halide fluorides and iodides are around $\langle r^2\rangle^{1/2} \approx 100$ nm,[17,18] and a similar order of magnitude can be expected for chloride perovskites.

When the thermalization length exceeds the Onsager radius, trapping processes become dominant and determine the course of luminescence quenching. This means that at elevated temperatures, already around 45 K, where the electron thermalization length ($\langle r^2\rangle^{1/2} \approx 100$ nm) is comparable to the Onsager radius (R_{Ons} = 100 nm), the contribution to exciton luminescence quenching is governed by recombination of stochastic charge carriers at non-radiative defects. Based on the above, it can be assumed that for pristine $CsPbCl_3$, one of the quenching mechanisms of the integrated exciton luminescence intensity is the escape of electrons beyond the Onsager sphere, with an activation energy of 39 meV, which is lower than the exciton binding energy of 64 meV. Considering that the Onsager radius decreases in the presence of activator dopants,[17] it can be expected that luminescence quenching *via* electron trapping at defects will occur at lower activation barriers. Accordingly, in $CsPbCl_3$:Sr (1 mol%) crystals, the activation energy for luminescence quenching is lower and equals 30 meV.

The difference between the activation barrier (14 meV) for the quenching of near edge luminescence and the exciton binding energy (39 meV) was observed in the $CsPbBr_3$ crystal and was explained in terms of an increased probability for electron excitations to escape the Onsager sphere[20] due to the reduction of the Onsager sphere size with increasing temperature.

3.2.2. Decay time parameters. The luminescence decay curves in the temperature range of 10–150 K are presented for $CsPbCl_3$ in Fig. 9 (Fig. S5) and for $CsPbCl_3$:Sr (1 mol%) in Fig. 10 (Fig. S6). The decay curves exhibit a general trend of decreasing decay time constants with increasing sample temperature. The average decay constants, τ_{av}, vary approximately

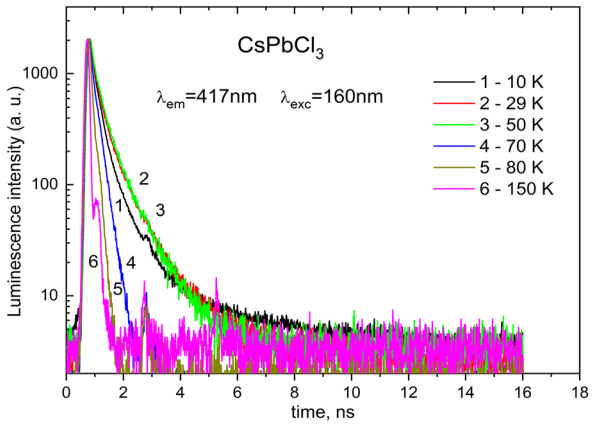

Fig. 9 Luminescence decay curves of the 417 nm luminescence band of the $CsPbCl_3$ single crystal at different temperatures under excitation with a light of $h\nu_{exc}$ = 7.75 eV (λ_{exc} = 160 nm).

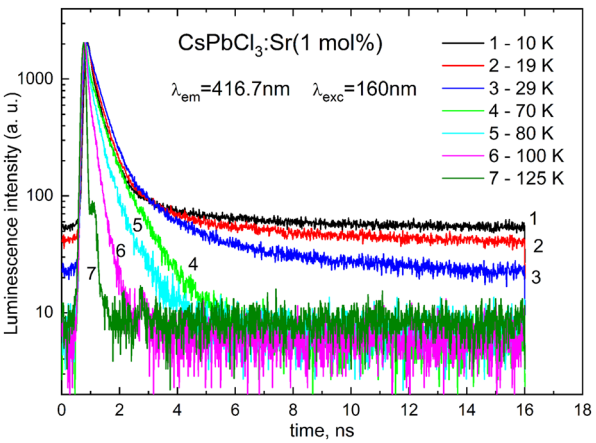

Fig. 10 Luminescence decay curves of the 416.7 nm luminescence band of the $CsPbCl_3$:Sr (1 mol%) single crystal at different temperatures under excitation with a light of $h\nu_{exc}$ = 7.75 eV (λ_{exc} = 160 nm).

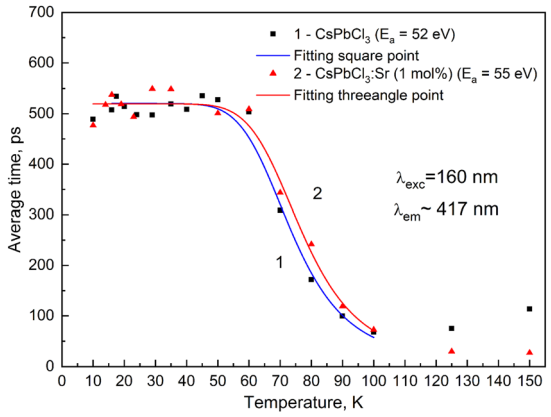

Fig. 11 Temperature dependence of the luminescence decay constants for the 417.2 nm band of the $CsPbCl_3$ single crystal (squares, curve 1 – approximation of experimental data) and the 416.5 nm band of the $CsPbCl_3$:Sr (1 mol%) single crystal (triangles, curve 2 – approximation of experimental data). Excitation: $h\nu_{exc}$ = 7.75 eV (λ_{exc} = 160 nm).

from τ_{av} = 500 ps (T = 10 K) to τ_{av} = 60 ps (T = 120 K). The decay time constants for the doped crystals are slightly higher than those for the undoped crystals. It should be noted that the decay curves of $CsPbCl_3$:Sr (1 mol%) (Fig. 10) display a larger background contribution, particularly in the temperature range of 10–30 K, which arises not from the photomultiplier dark current but rather from a slow decay component perceived as the background, attributable to the involvement of traps in the recombination luminescence.

The temperature dependence of the decay time constants shown in Fig. 11 differs from the temperature dependence of the luminescence intensity presented in Fig. 8. While the luminescence intensity decreases with increasing temperature, the decay time constants remain nearly constant in the temperature range of 10–60 K. This behavior is observed for both the undoped and the doped $CsPbCl_3$ crystals.

We assume that the luminescence quenching occurs *via* two mechanisms: (i) the escape of electron excitations from the Onsager sphere followed by recombination with defects, and (ii) the thermal dissociation of excitons. The first process does not affect the kinetic parameters, as the electron excitations are captured by defects before exciton formation. Therefore, only processes associated with the thermal dissociation of excitons contribute to the temperature dependence of the decay time constants. Accordingly, the activation energies E_a, obtained from the analysis of the temperature dependence of the decay time constants

$$\tau(T) = \frac{\tau_0}{(1 + B \cdot \exp(-E_a/kT))}, \quad (4)$$

can be expected to be close to the exciton binding energy (τ_0 – the decay time constant in the absence of exciton dissociation).

For the undoped $CsPbCl_3$ crystal, the activation energy is (52 ± 4) meV, whereas for $CsPbCl_3$:Sr (1 mol%), it is (55 ± 5) meV, which is slightly lower than the exciton binding energy (64 meV). Within the experimental uncertainty, the activation energy (*i.e.*, the exciton binding energy) appears to be insensitive to the Sr concentration of 1 mol%.

The influence of Sr on the thermal activation energy has been analyzed in terms of changes in exciton binding energy, using the band structure of the crystals. According to quantum-mechanical calculations for 12.5% Sr doping, the band gap increases by 0.3 eV, and the band dispersion is altered, leading to a decrease in the effective mass of charge carriers and the reduced mass of excitons. The reduced exciton mass results in a lower exciton binding energy. Calculations indicate a trend toward reduced exciton binding energy upon Sr incorporation (see the SI, Chapter 3: Exciton binding energy). For 12.5% Sr, the exciton binding energy is 31 meV in Sr-doped $CsPbCl_3$ compared to 69 meV for pristine $CsPbCl_3$ (Table S2). Experimentally, this would manifest as a reduction in the thermal activation energy for exciton luminescence quenching. F 1% Sr, the thermal activation energy E_a = (52 ± 4) meV coincides with E_a = (55 ± 5) meV for the pristine crystal within experimental error. This result can be explained by the fact that at 1% Sr concentration, the electron energy band structure and,

consequently, the band dispersion do not undergo significant changes, as the position of the main exciton peak in Sr-doped $CsPbCl_3$ (416.7 nm) remains almost unchanged compared to that in the pristine crystal (416.9 nm).

4. Conclusions

The activation of $CsPbCl_3$ crystals with Sr dopants leads to modification of the near edge luminescence spectrum, resulting in the appearance of additional exciton-like bands and their shift toward the high-energy region. These additional exciton-like bands may arise from the scattering of excitons at defects introduced by the Sr dopants. The blue shift of the emission bands can be associated with changes in the lattice parameters and modifications of the conduction band of $CsPbCl_3$, specifically through the mixing of 5s and 3d states of Sr^{2+} with 6p states of Pb^{2+} at the bottom of the conduction band. Another outcome of Sr^{2+} activation in $CsPbCl_3$ crystals is a pronounced increase in the near edge luminescence intensity (by nearly an order of magnitude), which is attributed to the improved ordering of the host lattice and the reduced concentration of chlorine and lead vacancies that act as traps for excitons. The temperature-dependent quenching of the integrated near edge luminescence under high-energy excitation is ascribed to the escape of electrons during thermalization from the Onsager sphere, where they can recombine non-radiatively at defects. The activation energies, determined from the temperature dependence of the decay time constants of the near edge luminescence, are close to the exciton binding energies. The observed increase in the edge luminescence intensity of the doped $CsPbCl_3$ crystals indicates their potential for application as fast scintillators, with $\tau_1 \approx 200$ ps at low temperatures.

Author contributions

A. P: investigation, writing – original draft, and writing – review & editing. O. P: investigation, formal analysis, and visualization. Ya. C: software. T. M: formal analysis and visualization. T. D: investigation, visualization, and writing – original draft. O. A: resources and investigation. V. St: visualization. V. Sa: resources. R. G: investigation. O. B: software. A. Z: investigation. Y. S: methodology and investigation. A. K: methodology and investigation. A. V: conceptualization, writing – original draft, writing – review & editing, and supervision. The manuscript has been read and approved by all listed authors.

Conflicts of interest

No conflicts of interest arise by publishing this work.

Data availability

The data supporting this article are provided in the Supplementary information (SI). Supplementary information includes: elemental composition of the samples, electronic band structure of the crystals, impurity formation energies in Sr-doped $CsPbCl_3$ crystals, exciton binding energies, chlorine vacancy formation energies, comparative luminescence spectra and luminescence decay curves at different temperatures. See DOI: https://doi.org/10.1039/d5tc03602j.

Acknowledgements

We acknowledge DESY (Hamburg, Germany), a member of the Helmholtz Association HGF, for the provision of experimental facilities carried out at PETRA III using beamline P66 operated by DESY Photon Science. Beamtime was allocated for the proposal I-20230140 EC. The research leading to this result was co-funded by the project NEPHEWS under Grant Agreement No. 101131414 from the EU Framework Programme for Research and Innovation Horizon Europe (T. D., R. G., A. P.). The work was partially supported by the Ministry of Education and Science of Ukraine (Grant No. 0125U002198) and has received funding through the EURIZON project, which is funded by the European Union under grant agreement no. 871072.

References

1 G. H. Ahmed, J. Yin, O. Bakr and O. Mohammed, Near-unity photoluminescence quantum yield in inorganic perovskite nanocrystals by metal-ion doping, *J. Chem. Phys.*, 2020, **152**, 020902, DOI: 10.1063/1.5131807.
2 Y. Chen, Y. Liu and M. Hong, Cation-Doping Matters in Caesium Lead Halide Perovskite Nanocrystals: from Physicochemical Fundamentals to Optoelectronic Applications, *Nanoscale*, 2020, **12**, 12228–12248, DOI: 10.1039/D0NR02922J.
3 G. H. Ahmed, J. El-Demellawi, J. Yin, J. Pan, D. B. Velusamy, M. Hedhili, E. Alarousu, O. Bakr, H. Alshareef and O. Mohammed, Giant Photoluminescence Enhancement in $CsPbCl_3$ Perovskite Nanocrystals by Simultaneous Dual-Surface Passivation, *ACS Energy Lett.*, 2018, **3**(10), 2301–2307, DOI: 10.1021/acsenergylett.8b01441.
4 N. Mondal, A. De and A. Samanta, Achieving Near-Unity Photoluminescence Efficiency for Blue-Violet-Emitting Perovskite Nanocrystals, *ACS Energy Lett.*, 2019, **4**(1), 32–39, DOI: 10.1021/acsenergylett.8b01909.
5 Q. Hu, J. Guo, M. Lu, P. Lu, Y. Zhang, W. William and X. Bai, Efficient and Stable Mg^{2+}-Doped $CsPbCl_3$ Nanocrystals for Violet LEDs, *J. Phys. Chem. Lett.*, 2021, **12**(34), 8203–8211, DOI: 10.1021/acs.jpclett.1c02416.
6 A. Erroi, F. Carulli, F. Cova, I. Frank, M. L. Zaffalon, J. Llusar, S. Mecca, A. Cemmi, I. D. Sarcina, F. Rossi, L. Beverina, F. Meinardi, I. Infante, E. Auffray and S. Brovelli, Ultrafast Nanocomposite Scintillators Based on Cd-Enhanced $CsPbCl_3$ Nanocrystals in Polymer Matrix, *ACS Energy Lett.*, 2024, **9**(5), 2333–2342, DOI: 10.1021/acsenergylett.4c00778.
7 A. Erroi, S. Mecca, M. L. Zaffalon, I. Frank, F. Carulli, A. Cemmi, I. D. Sarcina, D. Debellis, F. Rossi, F. Cova, K. Pauwels, M. Mauri, J. Perego, V. Pinchetti, A. Comotti,

F. Meinardi, A. Vedda, E. Auffray, L. Beverina and S. Brovelli, Ultrafast and Radiation-Hard Lead Halide Perovskite Nanocomposite Scintillators, *ACS Energy Lett.*, 2023, **8**, 3883–3894, DOI: 10.1021/acsenergylett.3c01396.0.

8 O. Pidhornyi, Ya Chornodolskyy, A. Pushak, Y. Smortsova, A. Kotlov, O. Antonyak, T. Demkiv, R. Gamernyk and A. Voloshinovskii, Enhancement of near edge luminescence in cadmium ions doped $CsPbCl_3$ single crystals, *J. Appl. Phys.*, 2023, **134**, 135105, DOI: 10.1063/5.0159753.

9 V. B. Mykhaylyk, M. Rudko, H. Kraus, V. Kapustianyk, V. Kolomiets, N. Vitoratou, Y. Chornodolskyy, A. S. Voloshinovskii and L. Vasylechko, Ultra-fast low temperature scintillation and X-ray luminescence of $CsPbCl_3$ crystals, *J. Mater. Chem. C*, 2023, **11**, 656–665, DOI: 10.1039/D2TC04631H.

10 J. J. van Blaaderen, D. Biner, K. W. Krämer and P. Dorenbos, The temperature dependent optical and scintillation characterisation of Bridgman grown $CsPbX_3$ (X = Br, Cl) single crystals, *Nucl. Instrum. Methods Phys. Res., Sect. A*, 2024, **1064**, 169322, DOI: 10.1016/j.nima.2024.169322.

11 Y. Smortsova, O. Chukova, M. Kirm, V. Nagirnyi, V. Pankratov, A. Kataeva and A. Kotlov, The P66 time-resolved VUV spectroscopy beamline at PETRA III storage ring of DESY, *J. Synchrotron Rad.*, 2025, **32**(6), 1539–1548, DOI: 10.1107/S1600577525007568.

12 J. A. Peters, Z. Liu, M. C. De Siena, M. G. Kanatzidis and B. W. Wessels, Defect levels in $CsPbCl_3$ single crystals determined by thermally stimulated current spectroscopy, *J. Appl. Phys.*, 2022, **132**(3), 035101, DOI: 10.1063/5.0091519.

13 M. Kovalenko, O. Bovgyra, Y. Chornodolskyy, O. Pidhornyi, A. Pushak and A. Voloshinovskii, Electronic Structure of Sr-doped $CsPbCl_3$ Crystal: First Principles Investigation, *Low Temp. Phys.*, 2025, **51**(3), 375–384, DOI: 10.1063/10.0035837.

14 M. Sebastian, J. A. Peters, C. C. Stoumpos, J. Im, S. S. Kostina, Z. Liu, M. G. Kanatzidis, A. J. Freeman and B. W. Wessels, Excitonic emissions and above-band-gap luminescence in the single-crystal perovskite semiconductors $CsPbBr_3$ and $CsPbCl_3$, *Phys. Rev. B: Condens. Matter Mater. Phys.*, 2015, **92**(23), 235210, DOI: 10.1103/PhysRevB.92.235210.

15 J. A. Peters, Z. Liu, M. C. de Siena, M. G. Kanatzidis and B. W. Wessels, Photoluminescence spectroscopy of excitonic emission in $CsPbCl_3$ perovskite single crystals, *J. Lumin.*, 2022, **243**, 118661, DOI: 10.1016/j.jlumin.2021.118661.

16 M. Baranowski, P. Plochocka, R. Su, L. Legrand, T. Barisien, F. Bernardot, Q. Xiong, C. Testelin and M. Chamarro, Exciton binding energy and effective mass of $CsPbCl_3$: a magneto-optical study, *Photonics Res.*, 2020, **8**(10), A50–A55, DOI: 10.1364/PRJ.401872.

17 A. N. Vasil'ev and A. V. Gektin, Multiscale Approach to Estimation of Scintillation Characteristics, *IEEE Trans. Nucl. Sci.*, 2014, **61**(1), 235–245, DOI: 10.1109/TNS.2013.2282117.

18 V. Vistovskyy, Ya Chornodolskyy, M. Chylii, V. Hevyk, S. Syrotyuk, A. Vas'kiv, A. Zhyshkovych and A. Voloshinovskii, Simulation of X-ray excited luminescence dependence on the size of MeF_2 (Me = Ba, Ca, Sr) nanoparticle, *Visn. Lviv Univ., Ser. Phys.*, 2015, **50**, 48–63.

19 V. V. Vistovskyy, A. V. Zhyshkovych, Ya. M. Chornodolskyy, O. S. Myagkota, A. Gloskovskii, A. V. Gektin, A. N. Vasil'ev, P. A. Rodnyi and A. S. Voloshinovskii, Self-trapped exciton and core-valence luminescence in BaF_2 nanoparticles, *J. Appl. Phys.*, 2013, **114**, 194306, DOI: 10.1063/1.4831953.

20 M. Dendebera, Y. Chornodolskyy, R. Gamernyk, O. Antonyak, I. Pashuk, S. Myagkota, I. Gnilitskyi, V. Pankratov, V. Vistovskyy, V. Mykhaylyk, M. Grinberg and A. Voloshinovskii, Time resolved luminescence spectroscopy of $CsPbBr_3$ single crystal, *J. Lumin.*, 2020, **225**, 117346, DOI: 10.1016/j.jlumin.2020.117346.